THE EXTENT OF POWER-LAW ENERGY SPECTRA IN COLLISIONLESS RELATIVISTIC MAGNETIC RECONNECTION IN PAIR PLASMAS

G. R. WERNER[1], D. A. UZDENSKY[1], B. CERUTTI[2,4], K. NALEWAJKO[3,5,6], AND M. C. BEGELMAN[3,7]

[1] Center for Integrated Plasma Studies, Physics Department, 390 UCB, University of Colorado, Boulder, CO 80309, USA; Greg.Werner@colorado.edu
[2] Department of Astrophysical Sciences, Princeton University, Princeton, NJ 08544, USA
[3] JILA, University of Colorado and National Institute of Standards and Technology, 440 UCB, Boulder, CO 80309-0440, USA

ABSTRACT

Using two-dimensional particle-in-cell simulations, we characterize the energy spectra of particles accelerated by relativistic magnetic reconnection (without guide field) in collisionless electron–positron plasmas, for a wide range of upstream magnetizations σ and system sizes L. The particle spectra are well-represented by a power law $\gamma^{-\alpha}$, with a combination of exponential and super-exponential high-energy cutoffs, proportional to σ and L, respectively. For large L and σ, the power-law index α approaches about 1.2.

Key words: acceleration of particles – galaxies: jets – gamma-ray burst: general – magnetic reconnection – pulsars: general – relativistic processes

1. INTRODUCTION

Magnetic reconnection is a fundamental plasma physics process in which magnetic field rearrangement and relaxation rapidly converts magnetic energy into particle energy (Zweibel & Yamada 2009). Reconnection is believed to drive many explosive phenomena in the universe, from Earth magnetospheric substorms and solar flares to high-energy X-ray and γ-ray flares in various astrophysical objects. Quite often, the radiation spectra of these flares, and hence the energy distributions of the emitting particles, are observed to be nonthermal (e.g., characterized by power laws). Therefore, understanding the mechanisms of *nonthermal particle acceleration* and determining the observable characteristics—such as the power-law index and high-energy cutoff—of the resulting particle distribution, is an outstanding problem in modern heliospheric physics and plasma astrophysics.

Of particular interest in high-energy astrophysics is the role of *relativistic reconnection*—which occurs when the energy density of the reconnecting magnetic field, $B_0^2/8\pi$, exceeds the rest-mass energy density $n_b mc^2$ of the ambient plasma, leading to relativistic bulk outflows and plasma heating to relativistic temperatures—as a potentially important mechanism for nonthermal particle acceleration to ultra-relativistic energies (with Lorentz factors $\gamma \gg 1$) in various astrophysical sources (Hoshino & Lyubarsky 2012). In particular, this process has been invoked to explain energy dissipation and radiation production in electron–positron (pair) plasmas over multiple scales in pulsar systems—e.g., in the pulsar magnetosphere near the light cylinder, in the striped pulsar wind, and in the pulsar wind nebula (PWN; Coroniti 1990; Lyubarsky 1996; Lyubarsky & Kirk 2001; Sironi & Spitkovsky 2011; Uzdensky et al. 2011; Cerutti et al. 2012a, 2013, 2014a, 2014b; Uzdensky & Spitkovsky 2014). In addition, relativistic reconnection in pair and/or electron–ion plasmas is believed to play an

important role in gamma-ray bursts (GRBs; Drenkhahn & Spruit 2002; Giannios & Spruit 2007; McKinney & Uzdensky 2012) and in coronae and jets of accreting black holes, including active galactic nucleus (AGN)/blazar jets, e.g., in the context of TeV blazar flares (Giannios et al. 2009; Nalewajko et al. 2011).

Nonthermal particle acceleration is essentially a kinetic (i.e., non-fluid) phenomenon. Although fluid simulations with test particles have been used to study particle acceleration, particle-in-cell (PIC) simulations include kinetic effects self-consistently. A number of PIC studies have investigated particle acceleration in collisionless relativistic pair-plasma reconnection (Zenitani & Hoshino 2001, 2005, 2007, 2008; Jaroschek et al. 2004; Lyubarsky & Liverts 2008; Liu et al. 2011; Sironi & Spitkovsky 2011; Bessho & Bhattacharjee 2012; Cerutti et al. 2012a, 2013, 2014a, 2014b; Kagan et al. 2013, 2015; Liu et al. 2015); the best evidence for nonthermal particle distributions was provided recently by Sironi & Spitkovsky (2014), Guo et al. (2014). Whereas previous studies have identified *power-law slopes* of nonthermal spectra, the important question of the energy *extent* of these power laws has not been systematically addressed.

In this letter we present a comprehensive two-dimensional (2D) PIC investigation of non-thermal particle acceleration in collisionless relativistic reconnection in a pair plasma without guide magnetic field. In particular, we characterize the dependence of the resulting energy distribution function on the system size L and the upstream "cold" magnetization parameter $\sigma \equiv B_0^2/(4\pi n_b m_e c^2)$ (relativistic reconnection requires $\sigma \gg 1$). We find empirically that relativistic reconnection produces a high-energy spectrum that is well represented by a power law with exponential and super-exponential cutoffs:

$$f(\gamma) = \frac{dN}{d\gamma} \propto \gamma^{-\alpha} \exp\left(-\gamma/\gamma_{c1} - \gamma^2/\gamma_{c2}^2\right). \tag{1}$$

The different cutoffs serendipitously allow us to distinguish different scalings with σ and L: $\gamma_{c1} \sim 4\sigma$ depends on σ, while $\gamma_{c2} \sim 0.1\,L/\rho_0$ depends on L (here $\rho_0 \equiv m_e c^2/eB_0$ is the nominal Larmor radius).
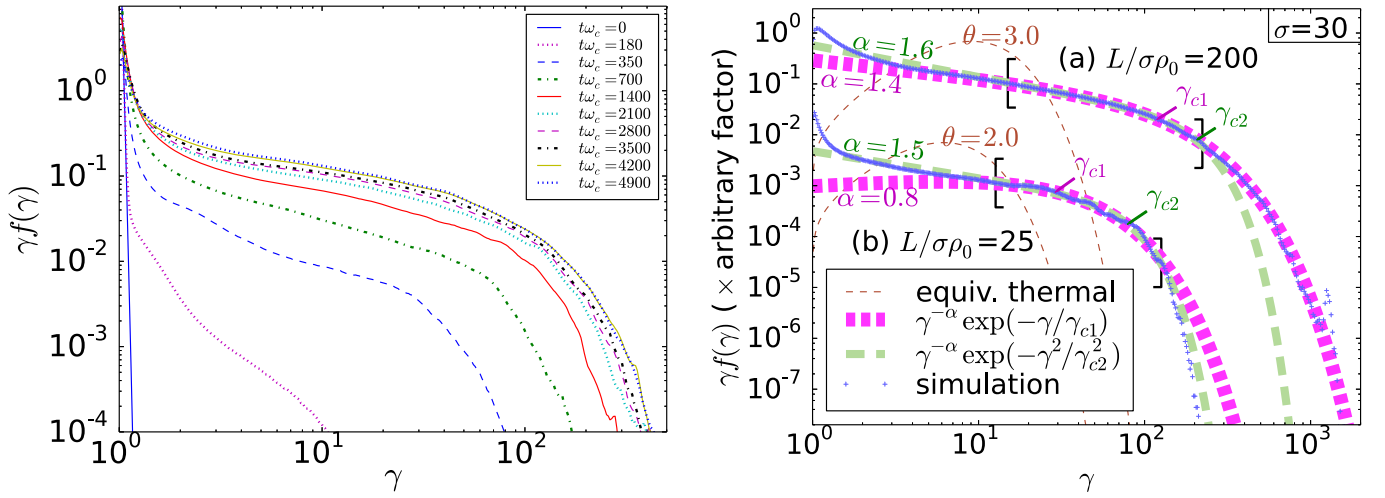
Equality of the two cutoffs, $\gamma_{c1} \simeq \gamma_{c2}$, defines a critical size $L_c \simeq 40\sigma\rho_0$ separating the small- and large-system regimes.

Figure 1. (Left) Time evolution of the particle energy spectrum for a run with $\sigma = 30$ and $L/\sigma\rho_0 = 200$. Reconnection ceases at $t\omega_c \approx 4300$, but the shape of the high-energy spectrum is the same for $t\omega_c \gtrsim 2000$ [$\omega_c \equiv c/(\theta_d\rho_0)$]. (Right) An exponential cutoff (short dashes) fits the energy spectra better for large-L simulations (a), while a super-exponential cutoff (long dashes) fits better for small L (b). Brackets mark $[\gamma_{f1}, \gamma_{f2}]$, where the displayed fits were performed. Thin-dashed lines show Maxwell–Jüttner distributions with equivalent total energies. Considering many fits (e.g., with different γ_{f1}, γ_{f2}), we determined for (a) $\alpha \in [1.38, 1.49]$, $\gamma_{c1} \in [119, 157]$, γ_{c2} too large/uncertain to measure; for (b) $\alpha \in [1.31, 1.48]$, γ_{c1} too large/uncertain to measure, $\gamma_{c2} \in [39, 44]$.

We find that for large systems ($L/\sigma\rho_0 \gg 40$), the energy spectrum of accelerated particles (hence γ_{c1}) is essentially independent of L. Importantly (as we discuss later), L_c is approximately the length at which a current layer, with thickness equal to the average Larmor radius $\rho_e = \bar{\gamma}\rho_0$, becomes tearing-unstable and breaks up into multiple plasmoids and secondary current sheets. (Here, $\bar{\gamma}m_ec^2$ is the average dissipated energy per background particle, $\bar{\gamma} \simeq \kappa(B_0^2/8\pi)/(n_bm_ec^2) = \kappa\sigma/2$; in our simulations $\kappa \simeq 0.6$, so $\bar{\gamma} \simeq 0.3\sigma$.) Therefore, we propose that (at least in 2D with an initially cold background plasma) reconnection in the plasmoid-dominated regime yields a high-energy particle spectrum that is predominantly independent of system size $L \gg L_c$. Consequently, nonthermal particle acceleration in *huge*, astrophysically relevant systems may be studied via merely *large* simulations, i.e., with $L \gtrsim L_c$.

2. SIMULATIONS

This study focuses on reconnection in 2D without guide field ($B_z = 0$). Although some important differences in the reconnection dynamics emerge between 2D and 3D, such as the development of the drift-kink instability (Zenitani & Hoshino 2008), the dimensionality is not believed to affect the particle energy spectra at late stages (W. Daughton 2014, private communication; J. F. Drake 2014, private communication; Guo et al. 2014; Sironi & Spitkovsky 2014). Working in 2D (much less costly than 3D) enabled investigation of large system sizes.

We simulate systems of size $L_x = L_y = L$ with periodic boundary conditions and two antiparallel reconnection layers. The two layers begin as relativistic Harris current sheets (Kirk & Skjæraasen 2003) with upstream magnetic field $B_x = B_0$ and a peak drifting plasma simulation-frame-density n_d (at the layer centers) that is 10 times the uniform background density n_b. A small (1%) initial magnetic-flux perturbation facilitates reconnection onset. Electrons and positrons in each Harris layer drift (in opposite directions) with average velocity $\beta_dc = 0.6c$, and initial Maxwell–Jüttner temperature $\theta_d \equiv k_BT_d/m_ec^2 = \sigma/16$; the initial layer half-thickness is $\delta = (8/3)\theta_d\,\rho_0 = \sigma\rho_0/6$. The background plasma is initially at rest, with temperature $\theta_b \ll \sigma$;

however, due to the finite grid instability (Birdsall & Maron 1980), the background plasma is expected to heat until its Debye length is resolved, which occurs at a temperature of order $\theta_D \sim \sigma/512$ for $\Delta x = \sigma\rho_0/32$.

The simulations begin with $N_p = 128$ (macro)particles per grid cell with cell sizes $\Delta x = \Delta y = \theta_d\,\rho_0/2 = \sigma\rho_0/32 \approx 0.2\delta$ (except for $\sigma = 3$, where the mildly relativistic particles allowed $\Delta x = \theta_d\rho_0$ without sacrificing accuracy). The total energy is conserved within 1% during each simulation. Convergence tests with respect to Δx and N_p indicate that our simulations are well resolved and, in particular, that the high-energy parts of the particle distributions are robust.
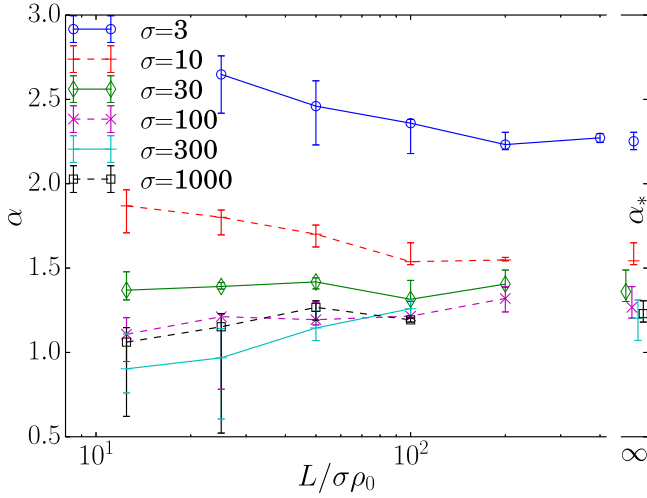
The Vorpal code (Nieter & Cary 2004), employed for this study, uses an explicit electromagnetic PIC time advance, with Yee electromagnetics and a relativistic Boris particle push.

To determine the power-law index α and the energy cutoffs γ_{c1} and γ_{c2} as functions of the upstream magnetization σ and the system size L, we ran simulations with $\sigma = 3, 10, 30, 100, 300, 1000$, and, for each σ, a range of system sizes up to $L/\sigma\rho_0 = 100$ for $\sigma = 1000, 300$, up to $L/\sigma\rho_0 = 200$ for $\sigma = 100, 30, 10$, and up to $L/\sigma\rho_0 = 400$ for $\sigma = 3$.

3. RESULTS

We focus on the energy distribution of background particles, excluding the initially drifting particles, which contribute negligibly to the overall distribution for large L. Evolution to a nonthermal distribution proceeds rapidly (Figure 1); and the shape of the high-energy spectrum, as characterized by α and $\gamma_{c1/2}$, ceases to evolve well before all available flux has reconnected, especially for large systems.

We find that the late-time high-energy spectrum is a power law with a high-energy cutoff significantly above the average particle energy, in agreement with Sironi & Spitkovsky (2014). We further observe (Figure 1) that spectra for large systems have exponential cutoffs, $\exp(-\gamma/\gamma_{c1})$, while small systems have sharper cutoffs, which we empirically model with a super-exponential $\exp(-\gamma^2/\gamma_{c2}^2)$. We therefore fit all spectra with the universal form of Equation (1) to determine the power-law index α and the cutoffs γ_{c1}, γ_{c2}; for small systems, the best-fit

Figure 2. Measured power-law indices α vs. L, with extrapolations (α_*) to $L \rightarrow \infty$ (cf. Figure 3).

Figure 3. Power-law index α_* vs. upstream magnetization σ.

γ_{c1} is typically much larger than γ_{c2} (hence irrelevant and highly uncertain), while for large L, γ_{c2} is larger and uncertain.

Each spectrum is fit to Equation (1) over an interval $[\gamma_{f1}, \gamma_{f2}]$, chosen as large as possible while maintaining a good fit. Because spectra depart from a power law at lowest energies, and because of increased noise at highest energies, larger fitting intervals yield unacceptably poor fits. Noise is reduced (and fit improved) by averaging over short time intervals and, if available, over multiple simulations (identical except for randomized initial particle velocities). Because the choices of acceptable fit quality and the durations of averaging intervals are somewhat subjective, we perform many fits using different choices, and finally report the median values with "error" bars encompassing the middle 68% of the fits (i.e., ± 1 standard deviation if the data were Gaussian-distributed); small error bars thus demonstrate insensitivity to the fitting process. Very uncertain and large (hence irrelevant) cutoff values are discarded.

By applying this fitting procedure to the background particle spectrum for each different value of (L, σ), we mapped out α, γ_{c1}, and γ_{c2} as functions of σ and L, up to sufficiently large L to estimate the asymptotic values $\alpha_*(\sigma) = \lim_{L \rightarrow \infty} \alpha(\sigma, L)$ (Figure 2). We find that $\alpha_*(\sigma)$ starts above 2 for modest σ, and decreases to $\alpha_*(\sigma) \approx 1.2$ in the ultra-relativistic limit of $\sigma \gg 1$ (Figure 3), a result that is broadly consistent with previous studies (Zenitani & Hoshino 2001; Jaroschek et al. 2004; Lyubarsky & Liverts 2008; Guo et al. 2014; Melzani et al. 2014; Sironi & Spitkovsky 2014); while our measurement is closer to 1.2 than 1, the uncertainty is too large to rule out $\alpha_* \rightarrow 1$, predicted by some (Larrabee et al. 2003; Guo et al. 2014).

In contrast to the power-law index α, the energy *extent* of the power law has received relatively little attention in relativistic reconnection literature (Larrabee et al. 2003; Lyubarsky & Liverts 2008). We find that the high-energy cutoffs scale as $\gamma_{c1} \sim 4\sigma$ (*independent of L*) and $\gamma_{c2} \sim 0.1 \, L/\rho_0$ (*independent of σ*) (Figures 4 and 5). Thus $L/\sigma\rho_0 \ll 40$ implies $\gamma_{c2} \ll \gamma_{c1}$, and a super-exponential cuts off the power-law at an energy determined by the system size. Larger system sizes $L/\sigma\rho_0 \gg 40$ have $\gamma_{c1} \ll \gamma_{c2}$, and so γ_{c1} determines where the power law ends, independent of L.
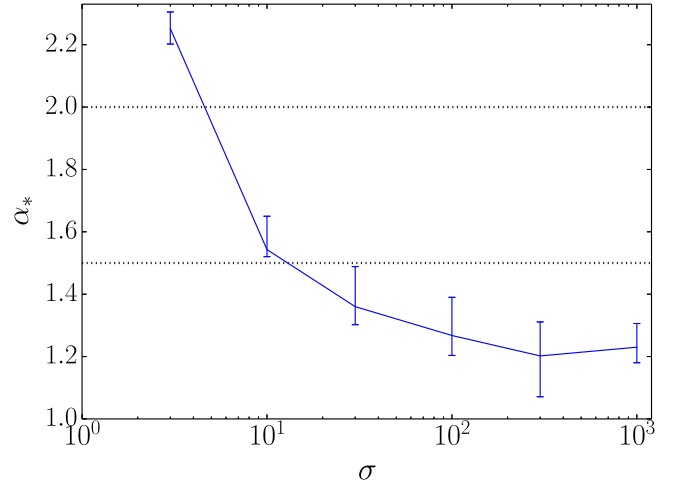
4. DISCUSSION

The scaling of the high-energy cutoffs can be explained in terms of the distance a particle could travel within the reconnection field $E_z \sim \beta_r B_0$ (where $\beta_r \sim 0.1$ is the reconnection rate). By calculating analytic trajectories in fields *around a single X-point*, (Larrabee et al. 2003) concluded that $f(\gamma) \propto \gamma^{-1} \exp(-\gamma/\Gamma_0)$ with $\Gamma_0 = 12e\beta_r^2 B_0 \ell_x / m_e c^2 \sim e E_z \ell_x / m_e c^2 \sim 0.1 \ell_x/\rho_0$, with ℓ_x being the size of the reconnection region in x,[8] a result that was supported by 2D PIC simulation in Lyubarsky & Liverts (2008).

In general, small systems reconnect mainly with one X-point, so $\ell_x \sim L$ and $\Gamma_0 \sim 0.1 \, L/\rho_0$, which equals our γ_{c2}. (The observed super-exponential form presumably results from the simulation's boundary conditions.)

In large systems, however, the tearing instability breaks up current layers with full-length greater than $\ell_{\text{tear}} \sim 100\bar{\delta}$, where $\bar{\delta}$ is the layer half-thickness (Loureiro et al. 2005; Ji & Daughton 2011), resulting in a hierarchy of layers ending with *elementary* layers, which are marginally stable against tearing (Shibata & Tanuma 2001; Loureiro et al. 2007; Uzdensky et al. 2010). The half-thickness of elementary (single X-point, laminar) layers should be about the average Larmor radius $\bar{\delta} \sim \rho_e = \bar{\gamma}\rho_0$ (Kirk & Skjæraasen 2003). Although Larrabee et al. (2003) considered single X-point reconnection, we propose that their formula for Γ_0 can also be used in the context of plasmoid-dominated reconnection in large systems if applied to elementary layers (instead of the entire global layer): $\ell_x \sim \ell_{\text{tear}} \sim 100\bar{\gamma}\rho_0 \sim 30\sigma\rho_0$ (instead of $\ell_x \sim L$). Then, $\Gamma_0 \sim 0.1\ell_{\text{tear}}/\rho_0 \sim 3\sigma$, which is essentially our γ_{c1} (and consistent with the measurement of $\Gamma_0 = 35$ for $\sigma = 9$ in Lyubarsky & Liverts 2008).

This explanation of high-energy-cutoff scaling in terms of elementary layer lengths may be robust despite the potentially important roles played by other acceleration mechanisms (Hoshino & Lyubarsky 2012). For example, significant additional acceleration may occur within contracting plasmoids (Drake et al. 2006; Dahlin et al. 2014; Guo et al. 2014, 2015) or—especially for the highest-energy particles—in the

---

[8] The x-extent of the reconnection region is the relevant length here because the calculation considered motion in the xz-plane subject to fields uniform in z, so escape (hence cessation of acceleration) was possible only through motion in x.
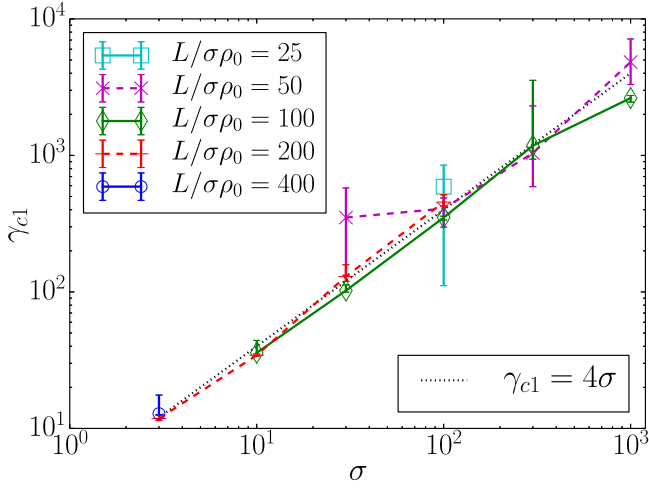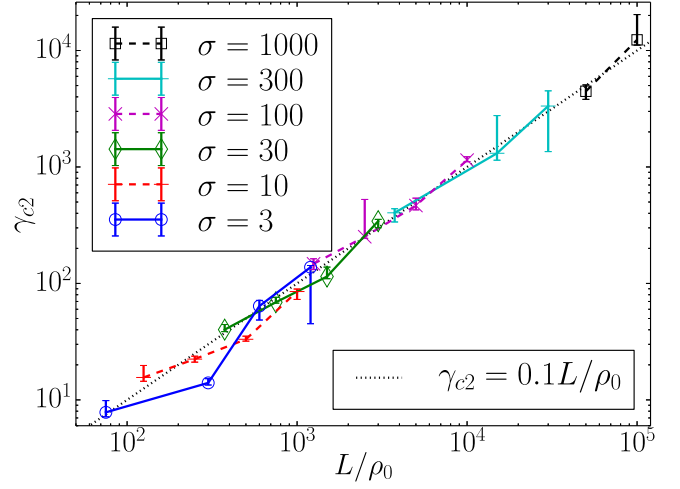
Figure 4. Exponential cutoff γ_{c1} scales linearly with magnetization σ.

Figure 5. Super-exponential cutoff γ_{c2} scales linearly with system size L.

(anti-)reconnection electric field of secondary plasmoid mergers (Oka et al. 2010; Sironi & Spitkovsky 2014; K. Nalewajko et al. 2015, in preparation).

It is interesting to compare our high-energy cutoffs to the upper bound imposed on a power-law distribution by a finite energy budget. When $1 < \alpha < 2$, most of the kinetic energy resides in high-energy particles, so the available energy per particle $\bar{\gamma} \sim 0.3\sigma$ limits the extent of the power law. If $f(\gamma) \sim \gamma^{-\alpha}$ extends from $\gamma_{\min}$ to $\gamma_{\max} \gg \gamma_{\min}$, then $\bar{\gamma} \approx [(\alpha - 1)/(2 - \alpha)]\gamma_{\min}^{\alpha-1}\gamma_{\max}^{2-\alpha}$ (Sironi & Spitkovsky 2014). For $\alpha \approx 1$, $\gamma_{\max}$ can extend well beyond $\bar{\gamma}$, but $\gamma_{\max}/\bar{\gamma}$ depends weakly on system parameters, consistent with our finding $\gamma_{c1} \sim \bar{\gamma} \sim \sigma$. E.g., for $\alpha = 1.2$, $\gamma_{\max}/\bar{\gamma} \approx (10^3\,\bar{\gamma}/\gamma_{\min})^{1/4}$. However, when $\alpha > 2$ (e.g., for low σ), the energy budget imposes no upper bound, since $\int_{\gamma_{\min}}^{\infty} \gamma\gamma^{-\alpha}d\gamma$ is finite. Nevertheless, for $\sigma = 3$ where $\alpha_* > 2$, we observe $\gamma_{c1} \sim 4\sigma$, the same as for smaller α_*.

The exponential cutoff at energies above $\gamma_{c1} \sim 4\sigma \sim 10\bar{\gamma}$ has important astrophysical implications for particle acceleration in systems such as pulsar magnetospheres, winds, PWN, and relativistic jets in GRBs and AGNs. Our results (insofar as they are ultra-relativistic) can be generalized to relativistically hot upstream plasmas by scaling all the energies by $\bar{\gamma}_b$, the average Lorentz factor of background particles. The "hot" magnetization $\sigma^{(\mathrm{hot})} \equiv B_0^2/(4\pi n w)$ therefore parameterizes similar simulations, since the relativistic specific enthalpy w also scales with $\bar{\gamma}_b$ (i.e., $w = \bar{\gamma}_b m_e c^2 + p_b/n_b$, where p_b is the background plasma pressure; for $\bar{\gamma}_b \gg 1$, $w \approx (4/3)\bar{\gamma}_b m_e c^2$).[9] For example, our reconnection-based model (Uzdensky et al. 2011; Cerutti et al. 2012a, 2013, 2014a, 2014b) for high-energy γ-ray flares in the Crab PWN (Abdo et al. 2011; Tavani et al. 2011) relies upon acceleration of a significant number of particles from $\bar{\gamma}_b \sim 3 \times 10^6$ to $\gamma \gtrsim 10^9$. If, to achieve this, we need $\gamma_{c1} > 10^9$, then direct extrapolation of the results from this letter would require $\sigma^{(\mathrm{hot})} \gtrsim (1/4)\gamma_{c1}/(w/m_e c^2) \approx 60$; this should be comparable (via scaling equivalence) to simulations presented in this work with $\sigma \sim 60$ (corresponding to a power-

law index $\alpha_* \sim 1.3$). This required $\sigma^{(\mathrm{hot})}$ is significantly higher than what is expected in the Crab Nebula. However, here we analyzed the entire spectrum of background particles, while (Cerutti et al. 2012b) suggested that bright flares observed in the Crab Nebula result from preferential focusing of the highest-energy particles into tight beams with energy spectra that differ from the entire spectrum. We also note that our present simulations are initialized with a Maxwellian plasma, whereas the ambient plasma filling the Crab Nebula has a power-law distribution, which may result in a higher high-energy cutoff.

5. CONCLUSION

We ran a series of collisionless relativistic pair-plasma magnetic reconnection simulations with no guide field, covering a wide range of system sizes L and upstream magnetizations $\sigma \geqslant 3$. We observed acceleration of the background plasma particles to a nonthermal energy distribution $f(\gamma) \sim \gamma^{-\alpha(L,\sigma)}$ with a high-energy cutoff. The cutoff energy is proportional to the maximum length of elementary, single X-point layers, which is limited by L in small systems, and by the secondary tearing instability in large systems. For small systems ($L \ll 40\sigma\rho_0$) we observe $f(\gamma) \sim \gamma^{-\alpha}\exp(-\gamma^2/\gamma_{c2}^2)$ with $\gamma_{c2} \sim 0.1\,L/\rho_0$, and for large systems, $f(\gamma) \sim \gamma^{-\alpha}\exp(-\gamma/\gamma_{c1})$ with $\gamma_{c1} \sim 4\sigma$. As L becomes large, the power-law index $\alpha(L, \sigma)$ asymptotically approaches $\alpha_*(\sigma)$, which in turn decreases to ≈ 1.2 as $\sigma \to \infty$. This characterization of power-law slope and high-energy cutoffs can be used to link ambient plasma conditions (i.e., σ) with observed radiation from high-energy particles, to investigate the role that reconnection plays in high-energy particle acceleration in the universe.

---

[9] Because the finite grid instability heats the background plasma until its Debye length is resolved (Birdsall & Maron 1980), the resolution prevents us from obtaining values of $\sigma^{(\mathrm{hot})}$ above a few hundred. For our simulations with $\sigma \lesssim 100$, $\sigma^{(\mathrm{hot})} \approx \sigma$; however, for $\sigma \gtrsim 300$, the numerical heating reduces the value of $\sigma^{(\mathrm{hot})}$.

REFERENCES

Abdo, A. A., Ackermann, M., et al. 2011, Sci, 331, 739
Bessho, N., & Bhattacharjee, A. 2012, ApJ, 750, 129
Birdsall, C. K., & Maron, N. 1980, JCoPh, 36, 1
Cerutti, B., Uzdensky, D. A., & Begelman, M. C. 2012a, ApJ, 746, 148
Cerutti, B., Werner, G. R., Uzdensky, D. A., & Begelman, M. C. 2012b, ApJL, 754, L33
Cerutti, B., Werner, G. R., Uzdensky, D. A., & Begelman, M. C. 2013, ApJ, 770, 147
Cerutti, B., Werner, G. R., Uzdensky, D. A., & Begelman, M. C. 2014a, PhPl, 21, 056501
Cerutti, B., Werner, G. R., Uzdensky, D. A., & Begelman, M. C. 2014b, ApJ, 782, 104
Coroniti, F. V. 1990, ApJ, 349, 538
Dahlin, J. T., Drake, J. F., & Swisdak, M. 2014, PhPl, 21, 092304
Drake, J., Swisdak, M., Che, H., & Shay, M. 2006, Natur, 443, 553
Drenkhahn, G., & Spruit, H. C. 2002, A&A, 391, 1141
Giannios, D., & Spruit, H. C. 2007, A&A, 469, 1
Giannios, D., Uzdensky, D. A., & Begelman, M. C. 2009, MNRAS, 395, L29
Guo, F., Li, H., Daughton, W., & Liu, Y.-H. 2014, PhRvL, 113, 155005
Guo, F., Liu, Y.-H., Daughton, W., & Li, H. 2015, ApJ, submitted (arXiv:1504.02193)
Hoshino, M., & Lyubarsky, Y. 2012, SSRv, 173, 521
Jaroschek, C. H., Treumann, R. A., Lesch, H., & Scholer, M. 2004, PhPl, 11, 1151
Ji, H., & Daughton, W. 2011, PhPl, 18, 111207
Kagan, D., Milosavljević, M., & Spitkovsky, A. 2013, ApJ, 774, 41
Kagan, D., Sironi, L., Cerutti, B., & Giannios, D. 2015, SSRv, 191, 545
Kirk, J. G., & Skjæraasen, O. 2003, ApJ, 591, 366
Larrabee, D. A., Lovelace, R. V. E., & Romanova, M. M. 2003, ApJ, 586, 72
Liu, W., Li, H., Yin, L., et al. 2011, PhPl, 18, 052105
Liu, Y.-H., Guo, F., Daughton, W., Li, H., & Hesse, M. 2015, PhRvL, 114, 095002
Loureiro, N. F., Cowley, S. C., Dorland, W. D., Haines, M. G., & Schekochihin, A. A. 2005, PhRvL, 95, 235003
Loureiro, N. F., Schekochihin, A. A., & Cowley, S. C. 2007, PhPl, 14, 100703
Lyubarsky, Y., & Kirk, J. G. 2001, ApJ, 547, 437
Lyubarsky, Y., & Liverts, M. 2008, ApJ, 682, 1436
Lyubarsky, Y. E. 1996, A&A, 311, 172
McKinney, J. C., & Uzdensky, D. A. 2012, MNRAS, 419, 573
Melzani, M., Walder, R., Folini, D., Winisdoerffer, C., & Favre, J. M. 2014, A&A, 570, A112
Nalewajko, K., Giannios, D., Begelman, M. C., Uzdensky, D. A., & Sikora, M. 2011, MNRAS, 413, 333
Nieter, C., & Cary, J. R. 2004, JCoPh, 196, 448
Oka, M., Phan, T.-D., Krucker, S., Fujimoto, M., & Shinohara, I. 2010, ApJ, 714, 915
Shibata, K., & Tanuma, S. 2001, EP&S, 53, 473
Sironi, L., & Spitkovsky, A. 2011, ApJ, 741, 39
Sironi, L., & Spitkovsky, A. 2014, ApJL, 783, L21
Tavani, M., Bulgarelli, A., et al. 2011, Sci, 331, 736
Uzdensky, D. A., Cerutti, B., & Begelman, M. C. 2011, ApJL, 737, L40
Uzdensky, D. A., Loureiro, N. F., & Schekochihin, A. A. 2010, PhRvL, 105, 235002
Uzdensky, D. A., & Spitkovsky, A. 2014, ApJ, 780, 3
Zenitani, S., & Hoshino, M. 2001, ApJL, 562, L63
Zenitani, S., & Hoshino, M. 2005, ApJL, 618, L111
Zenitani, S., & Hoshino, M. 2007, ApJ, 670, 702
Zenitani, S., & Hoshino, M. 2008, ApJ, 677, 530
Zweibel, E. G., & Yamada, M. 2009, ARA&A, 47, 291